AAAS
Ultrafast Science
Volume 2022, Article ID 9853053, 7 pages
https://doi.org/10.34133/2022/9853053

Ultrafast Science
A SCIENCE PARTNER JOURNAL

Research Article

Anti-Correlated Plasma and THz Pulse Generation during Two-Color Laser Filamentation in Air

Zhiqiang Yu,[1,2] **Lu Sun**,[1,2] **Nan Zhang**,[1,2] **Jianxin Wang**,[1,2] **Pengfei Qi**,[1,3] **Lanjun Guo**,[1,3] **Quan Sun**,[4,5] **Weiwei Liu**,[1,2] **and Hiroaki Misawa**[4,6]

[1]*Institute of Modern Optics, Nankai University, Tianjin 300350, China*
[2]*Tianjin Key Laboratory of Micro-scale Optical Information Science and Technology, Tianjin 300350, China*
[3]*Tianjin Key Laboratory of Optoelectronic Sensor and Sensing Network Technology, Tianjin 300350, China*
[4]*Research Institute for Electronic Science, Hokkaido University, Sapporo 001-0021, Japan*
[5]*Peking University Yangtze Delta Institute of Optoelectronics, Nantong, 226010 Jiangsu, China*
[6]*Center for Emergent Functional Matter Science, National Chiao Tung University, Hsinchu 30010, China*

Correspondence should be addressed to Quan Sun; sunquan@ydioe.pku.edu.cn and Weiwei Liu; liuweiwei@nankai.edu.cn

Received 15 April 2022; Accepted 24 July 2022; Published 5 August 2022

The THz generation efficiency and the plasma density generated by a filament in air have been found anti-correlated when pumped by 800 nm + 1600 nm two-color laser field. The plasma density near zero delay of two laser pulses has a minimum value, which is opposite to the trend of THz generation efficiency and contradicts common sense. The lower plasma density cannot be explained by the static tunneling model according to the conventional photocurrent model, but it might be attributed to the electron trapping by the excited states of nitrogen molecule. The present work also clarifies the dominant role of the drifting velocity accelerated by the two-color laser field during the THz pulse generation process. The results promote our understanding on the optimization of the THz generation efficiency by the two-color laser filamentation.

1. Introduction

In the past decades, terahertz (THz) pulse generated by the interaction between femtosecond laser pulse and gas plasma, i.e., filament, has attracted broad attention owing to its advantages of ultrabroad band and high field strength [1–3]. In order to coherently control the output THz wave, two-color laser (TCL) field, commonly synthesized by a Ti: sapphire femtosecond laser pulse (FL) centered around 800 nm and its second harmonic (SH), is frequently used as the pumping source [4–9]. In common sense, the superposition of two laser pulses will not only enhance the free electron density inside a filament [10], but also boost the efficiency of the THz wave generation [11–16]. The terahertz field strength strongly depends on the laser wavelength and relative phase between the two-color laser beams. When the time delay of the two-color field is close to zero delay, the phase difference is $\pi/2$, which increases the magnitude of the net current, thereby realizing strong terahertz wave radiation [17]. The cross-section of the THz wave generated by the dual-color laser filamentation is Gaussian distribution [18], and the beam divergence angle can be adjusted by changing the diameter and length of the plasma. Recent studies on THz generation using two-color lasers demonstrate that, as the pump laser energy increases, the THz generation energy increases, and when the laser energy continues to increase, secondary ionization occurs, and the THz intensity continues to increase [18–20]. Finally, due to intensity clamping and THz energy reabsorption in plasmas, the THz energy tends to saturation. In addition, researchers also use longer pump wavelength, transparent dielectric tape target to enhance the radiation of THz wave [19, 20]. Besides, increasing the plasma density is also reported an important method to improve the THz generation efficiency [5]. However, there are few experimental reports on the plasma density of the two-color laser filamentation that radiates THz. In the present work, the anticorrelation between the terahertz wave generation efficiency and the plasma density found in the 800 + 1600 nm two-color laser filamentation experimental breaks the cognition that the

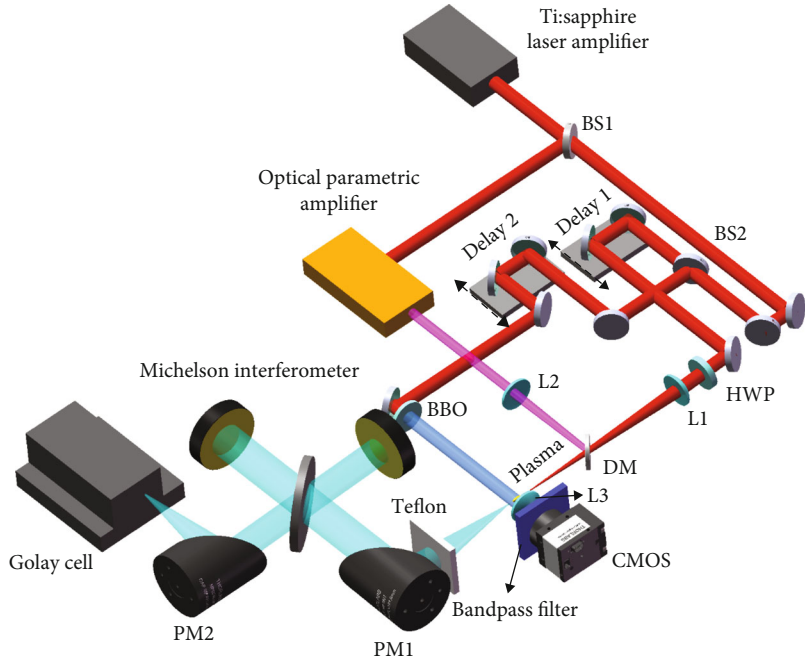

FIGURE 1: Scheme of the experimental setup. HWP: half-wave plate; L1-L3: lens; DM: dichromatic mirror; PM1, PM2: parabolic mirrors.

superposition of the two laser pulses would increase the free electron density and the efficiency of terahertz wave generation simultaneously.

In the current work, the variation of the THz amplitude generated by TCL in air has been studied as a function of the temporal delay between two laser pulses, which were centered around 800 nm and 1600 nm, respectively. At the same time, the plasms density generated by TCL has also been characterized. Surprisingly, the experimental results demonstrate an anti-correlation between the THz amplitude and the plasma density. THz amplitude reaches the maximum when there is zero delay between the two laser pulses, while the free electron density was recorded minimum, contrary to common sense. Our finding might provide new insight into the underlying mechanism of THz generation by TCL.

2. Experiment Setup

Figure 1 shows the schematic diagram of our experimental setup. During the experiments, a 1 kHz Ti: sapphire femtosecond amplifier (Solstice, Spectra Physics Inc.) which delivered 35 fs pulses with a central wavelength of 800 nm was employed. The pulse with a total energy of 5 mJ was split into two paths by a beam splitter (BS1). One path with 3 mJ pulse energy was used to pump an optical parametric amplifier (OPA, TOPAS), producing the pulse (POPA) whose wavelength can be tunable from 1200 nm to 1600 nm.

The other path was further divided into two beams by the second beam splitter (BS2). The main pulse (P_{FL}) was combined with the OPA output P_{OPA} by a dielectric mirror, yielding a filament in air. Two identical lenses (L1, L2), whose focal lengths were f = 100 mm, were used to focus two lasers before reaching DM. The laser beam radiuses ($1/e^2$) of P_{FL} and P_{OPA} on the front surface of the focusing lens were 4 mm and 2 mm, respectively. The polarizations of two pumping lasers were set to be parallel by using an air-space zero-order half-wave plate (HWP). An off-axis parabolic mirror was used to collect and collimate the forward propagation of the THz pulse emitted by the air plasma. The THz pulse energy was characterized by a Golay cell detector (GC-1P, Tydex Inc.), which was equipped with a 6-mm diameter high-density polyethylene input window. Note that in order to detect the THz pulses using the Golay cell, the femtosecond laser beam output from the laser systems was modulated by a chopper with a frequency of 15 Hz. Four pieces of 2-mm-thick Teflon plates were placed behind the filament to block the femtosecond laser and the stray light, which guaranteed that only the THz radiation can be detected by the Golay cell. Furthermore, the first-order autocorrelation of the THz pulse was measured by using a homemade Fourier spectrometer based on a Michelson interferometer as shown in Figure 1. The spectrum of the THz pulse was obtained by Fourier transforming the autocorrelation trace.

Another beam passed through a 100 μm thick type-I beta barium borate (BBO) crystal. The generated SH pulse (P_{SH}) was implemented as the probe of a shadow-graphic setup [21]. In detail, the SH beam propagated through the plasma zone perpendicularly. The plasma was imaged by a lens with a focal length of 50 mm onto a CMOS camera (DCC1240C-HQ, Thorlabs Inc.). A band-pass filter (ZBPA400, Asahi Spectra Inc.), which has a high within the spectral range of 390 nm-410 nm, was used to prevent FL and most of the supercontinuum from entering the CMOS camera.

The time delays among P_{OPA}, P_{FL}, and P_{SH} were adjusted by two translation stages (PT1-Z8, Thorlabs Inc.). The delay time between P_{FL} and P_{OPA} is indicated as Δt_1 and Δt_2 refer to the delay time between P_{FL} and P_{SH}. When $\Delta t_1 < 0$ or $\Delta t_2 < 0$, P_{FL} lagged behind P_{OPA} or P_{SH}, respectively.

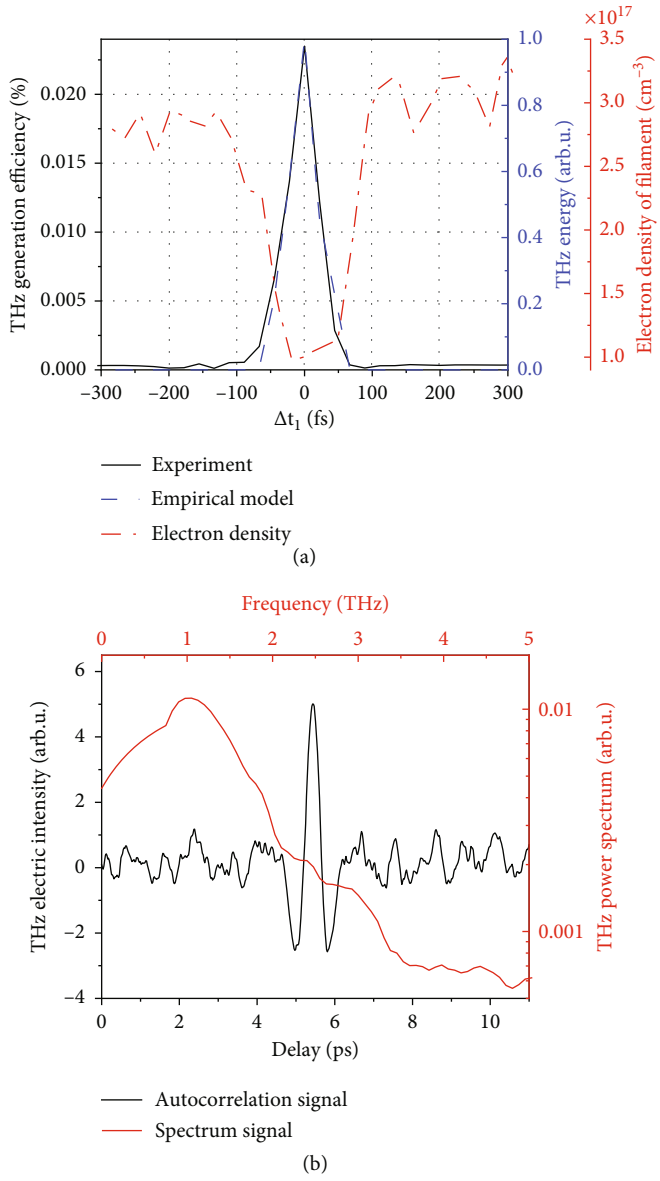

Figure 2: (a) Experimental and simulation results of THz yield as a function of Δt_1. The generated THz efficiency as a function of Δt_1 in the experiment is shown as the black solid line, while the simulated THz relative intensities of the empirical model is represented as blue dashed line. Free electron density with different retardations was measured on the filament axis at z = 2.7 mm and shown as red dash-dotted line. (b) The THz waveform autocorrelation trace and the THz spectrum in the experiment when $\Delta t_1 = 0$.

3. Results

3.1. Experimental Results. In Figure 2(a), the generated THz efficiency as a function of Δt_1 in the experiment is shown as the black solid line. Note that the single pulse energies of pump light and infrared light are 0.5 mJ and 0.3 mJ before the focusing lenses L1 and L2, respectively. It could be clearly seen that the THz energy has a maximum value near zero delay. The highest energy of the THz wave measured by the Golay cell detector is 188 nJ, and the corresponding THz conversion efficiency is 0.0235%. The THz waveform autocorrelation trace and the corresponding THz spectrum for $\Delta t_1 = 0$ are depicted in Figure 2(b).

Besides, the recorded shadowgraphs of the filament are shown in Figures 3(a)–3(c) for $\Delta t_1 = 400$ fs at different values of Δt_2. Worth mentioning that when $\Delta t_1 =$ 400 fs, there is no temporal overlap between P_{FL} and P_{OPA} as indicated in Figure 2(a). It could be seen that as Δt_2 increases, the filament becomes longer, which is mainly associated with the propagation of the fundamental pulse in air. However, the filament does not change significantly when Δt_2 is greater than 5000 fs, because the fundamental pulse has exceeded the filamentation zone. The shadowgraphs with different Δt_1 for $\Delta t_2 =$ 5000 fs were recorded to retrieve the variation of plasma density inside the filament. As an example shown in Figure 3(d), when Δt_1 is about zero, the absorption of the probe light after passing through the filament becomes weaker, and the filament becomes longer toward the lens.

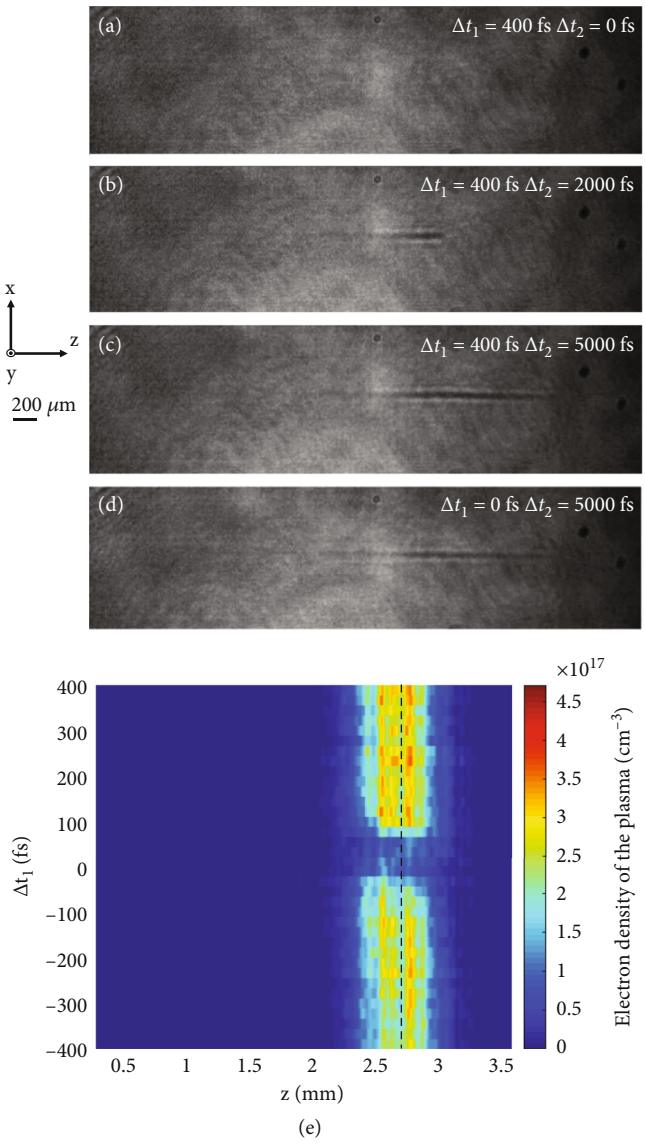

FIGURE 3: (a)–(d) Shadowgraphs recorded by a CMOS camera: (a)-(c) time-resolved shadowgraphs of femtosecond laser filament when Δt_1 is fixed at 400 fs and Δt_2 varies from 0 to 5000 fs; (d) Δt_1 and Δt_2 are set at 0 fs and 5000 fs, respectively. (e) Longitudinal distribution of on-axis free electron density of filament as a function of Δt_1 when Δt_2 = 5000 fs was calculated from Equation (1); dashed line corresponds to z = 2.7 mm.

3.2. Numerical Simulations. The plasma density was then deduced according to the absorption coefficient $\alpha = 1/d \ln(I_{p0}/I_{pd})$ as the follows [22]:

$$\begin{aligned} \alpha &= 2\omega\kappa/c \\ \varepsilon &= 1 - \omega_p^2\left[\frac{\tau^2}{(1+\omega^2\tau^2)} + \mathrm{i}\frac{\tau^2}{\omega\tau(1+\omega^2\tau^2)}\right] \\ \kappa &= \sqrt{\left(\sqrt{\varepsilon'^2 + \varepsilon''^2} - \varepsilon'\right)/2} \\ \omega_p &= \sqrt{e^2 N_e/m_e\varepsilon_0} \end{aligned}, \quad (1)$$

where d denotes the mean diameter of the filament, I_{p0} and I_{pd} represent the probe laser intensities before and after passing through the plasma. ω , κ, c, ε,ω_p, τ, ε', ε'', e, m_e, ε_0, and N_e correspond to the probe beam light frequency, the imaginary part of the refractive index of the air, the light speed in vacuum, the dielectric function, the real part of the dielectric function, the imaginary part of the dielectric function, the plasma frequency, the scattering time [23], the charge of electron, the electron's mass, the permittivity in vacuum, and the free electron density of plasma, respectively. Similar to the shading method, the filament fluorescence with different time delays was obtained during the experiment. When Δt_1 = 0 fs and 400 fs, Normalized fluorescence intensity distribution along the diameter of the filament is shown in Figure 4(a), and the full width at half maximum of the fluorescence intensity is almost the same. In addition, the diameters of the filaments with different time delays are basically the same, as shown in Figure 4(b). Therefore, the same diameter (d) can be substituted into the calculation.

Hence, the calculated free density at different Δt_1 is shown in Figure 3(e). In addition, the evolution of on-axis plasma density at z = 2.7 mm, which corresponds to the center of the filament, is highlighted in Figure 2(a) as the red dash-dotted line. Clearly, the plasma density on the filament has a minimum value when $\Delta t_1 = 0$, which is surprisingly opposite to the trend of THz generation efficiency shown in Figure 2(a).

Conventionally, THz wave generation by femtosecond laser filamentation could be explained by a photocurrent model [17]. In this scheme, the combined TCL field can be expressed as $E_L(t, \Delta t_1) = E_{\omega_1}\cos(\omega_1 t) + E_{\omega_2}\cos[\omega_2(t+\Delta t_1) + \theta]$, where E_{ω_1} and E_{ω_2} point to the amplitudes of the FL and the infrared light fields, respectively, ω_1 and ω_2 are the angular frequency of the FL and the infrared light, and θ denotes the initial relative phase between two fields. The ionization rate (per molecule) could be given by the static tunneling (ST) ionization model in the form:

$$W(t) = 4\omega_a\left(\frac{E_a}{E_L(t)}\right)\exp\left(-\frac{2}{3}\frac{E_a}{E_L(t)}\right), \quad (2)$$

where $\omega_a = 4.134 \times 10^{16} s^{-1}$ is the atomic frequency unit and $E_a = 5.14 \times 10^{11}$ V/m represents the atomic field of the ground state electron in a hydrogen atom. The yielded free electron density is maximum when Δt_1 is near zero, which is contrary to our experimental results [23].

The contradiction might be attributed to the reduced ionization by the 1600 nm laser induced by the resonance between the excited states. Though the influence of Rydberg states on multiphoton ionization remains unclear, previous studies have demonstrated that the intermediate states during ionization can trap excited electrons [17, 24]. Since nitrogen molecules dominate in the air, we focus on the electronic energy levels of nitrogen molecule which have been calculated based on the hybrid functional B3LYP and triple-zeta basis set aug-cc-pvtz [25, 26]. The electronic energy levels below $(E_{HOMO} + 15.6)$ eV are displayed in

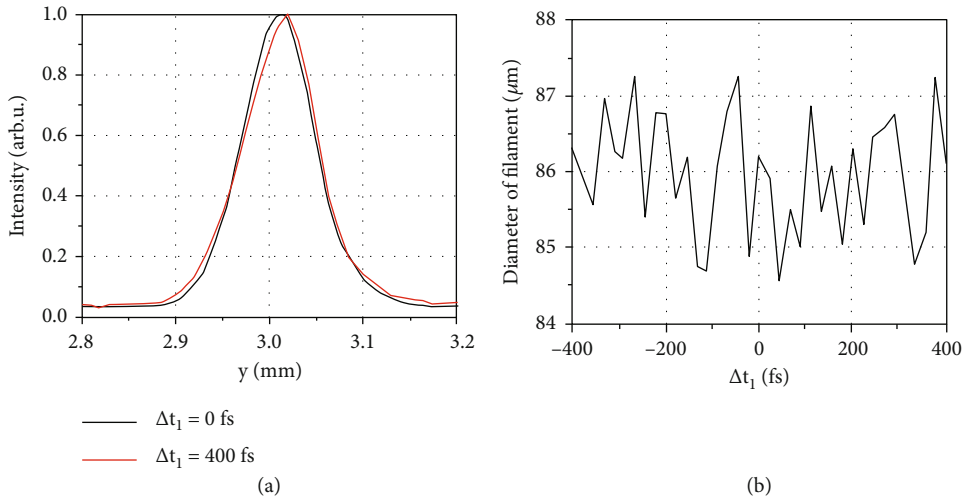

FIGURE 4: (a) Normalized fluorescence intensity distribution along the diameter of the filament (Δt_1 = 0 fs and 400 fs); (b) the diameter of the filaments measured with different time delays.

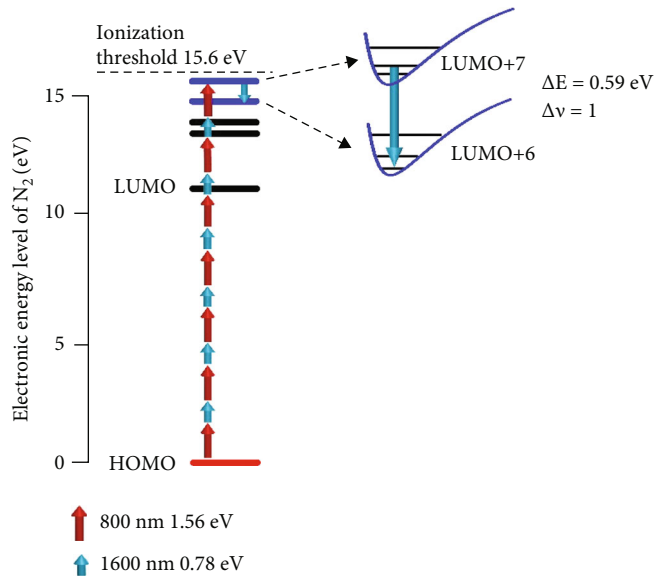

FIGURE 5: Calculated electronic energy level of nitrogen molecule. HOMO indicates the higher occupied molecular orbital, and LUMO indicates the lowest unoccupied molecular orbital. The photon energies corresponding to 800 nm and 1600 nm lasers are 1.56 and 0.78 eV, respectively. The vibration energy of nitrogen is about 0.2 eV. The energy gap that matches the energy of 1600 nm photon is colored blue, and the possible transitions between the gap are depicted on the right.

Figure 5. Note that 15.6 eV corresponds to the ionization energy of the nitrogen molecule.

In the case of dual-color field, the electron from HOMO is excited by 800 nm and 1600 nm photons shown in Figure 6. Since the energy of 1600 nm photon is 0.78 eV and the vibration energy of nitrogen is around 0.2 eV, resonance induced by 1600 nm photon is probable to occur when the electronic energy gap is around 0.78 ± 0.2 eV. Moreover, by analyzing the energy level, it is noted that the energy difference between HOMO and LUMO+7 is 15.47 eV. The value approximates the sum of seven 800 nm photons and six 1600 nm photons. Therefore, the electron can be excited to LUMO+7 orbital during ionization. Besides, the energy gap between LUMO+6 and LUMO+7 is 0.59 eV, implying that the resonance between the two levels can be induced by a 1600 nm laser and electron may be trapped, as shown in Figure 5. Thus, the decrease of the plasma density at zero delay might be attributed to the electron trapping by the excited states.

Since the two incident beams are Gaussian in the time domain, the experimentally measured plasma densities versus Δt_1 in Figure 2(a) can be fitted and expressed as

$$N(t) = 3 \times 10^{17} - 1 \times 10^{17} \exp\left(-\frac{\Delta t_1^2}{\tau^2}\right), \quad (3)$$

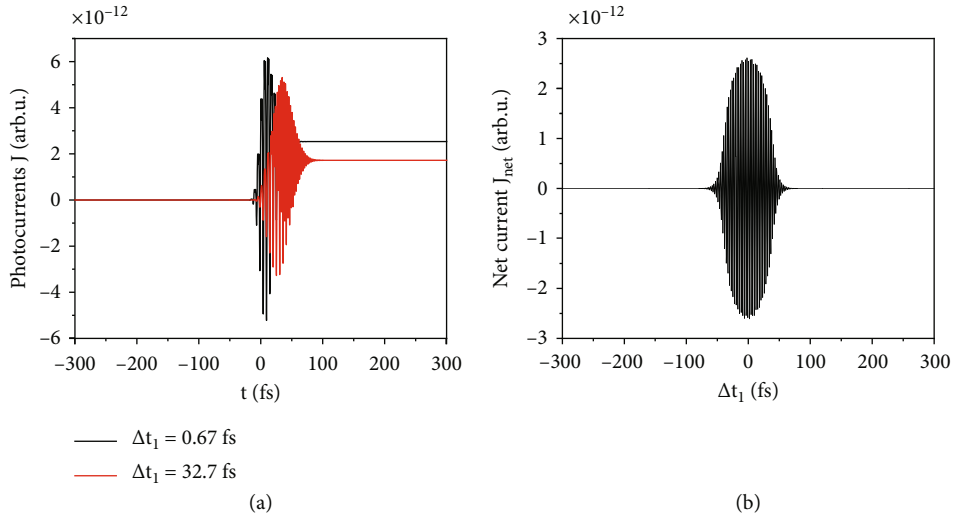

Figure 6: (a) Photocurrents $J(t)$ at $\Delta t_1 = 0.67$ fs and 32.7 fs, respectively. (b) Variation of net current J_{net} as a function of Δt_1.

where τ is the fitting parameter, about 85 fs. In order to understand the anti-correlation between the THz wave generation efficiency and plasma density, the underlying dynamic of THz wave generation has been studied according to the photocurrent model. The resulting transverse electron current can be written as

$$J(t) = -\int_{t_0}^{t} ev\left(t, t'\right) dN_e\left(t'\right), \tag{4}$$

where t_0 denotes the initial instant of the ionization process, *dNe(t')* represents the density of free electrons produced by the laser field in the interval between *t'* and *t'* + *dt'*, and *v(t,t')* refers to the drift velocity of those electrons at *t*. By substituting the experimental parameters such as laser center wavelength and electric field amplitude into Equation (4), the relative THz radiation intensities versus Δt_1 could be calculated.

However, since the conventional photocurrent model has failed in the explanation of the THz generation in our experiment, the description of the ionization dynamic, namely, ST model, has been replaced by an empirical model in the current work. The empirical model is modified on the basis of the traditional photocurrent model, the final plasma density obtained by the ST model at different time delays is replaced by the experimentally measured plasma density, and then the terahertz intensity is calculated by inversion. The resulted THz pulse energy is demonstrated in Figure 2(a) as the blue dashed line, which agrees well with the experimental outcome.

Furthermore, the temporal variation of $J(t)$ when $\Delta t_1 = 0.67$ fs and 32.7 fs are highlighted in Figure 6(a). It is essential to emphasize that the net current J_{net} determines the energy of the generated THz pulse in the framework of the photocurrent model [11, 12]. Figure 6(a) indicates that J_{net} depends on Δt_1, namely, the temporal delay between the fundamental laser pulse and the infrared laser pulse, strongly. Hence, the variation of J_{net} with respect to Δt_1 is also depicted in Figure 6(b). The oscillation period of the J_{net} is about 2.67 fs; however, due to the limitation of the translation stage precision during the experiment, only the envelope curve of the terahertz intensity can be obtained. Figure 6(b) implies that though the maximum free electron density inside the filament has minimum value when Δt_1 was small, $J_{net}(\Delta t_1)$ might reach the peak value, leading to the highest THz pulse energy. It should be attributed to the dominant role of the free electron acceleration by the laser pulse inside a filament according to Equation (4).

4. Conclusion

In conclusion, the collinear propagations of 1600 nm light and 800 nm light with different time delays are focused to form a filament in air. The free electron density inside the filament and the emitted THz pulse energy have been found anti-correlated, which contradicts the common sense of the community. The decrease of the plasma density at zero delay can be attributed to the electron trapping by the excited states. On the other hand, the drifting velocity accelerated by the two-color laser field has been confirmed to play a dominant role during the THz pulse generation process. The experiment results indicated the failure of the convention photocurrent model, which describes the ionization rate by using the static field model. In contrast, wavelength-dependent ionization model has to be taken into account. The results of the present work arouse the attention of the revisiting of the underlying dynamics of the THz generation by two-color laser filamentation, which has been paid broad research attention in the field of intensity THz wave generation.

Data Availability

The data that support the findings of this study are available from the corresponding authors upon reasonable request.

Conflicts of Interest

The authors declare that there is no conflict of interest regarding the publication of this article.

Authors' Contributions

Z. Q. Yu, L. Sun, and W. W. Liu performed the experiments. N. Zhang, J. X. Wang, and P. F. Qi performed the simulations and analyzed the data. L. J. Guo and H. Misawa contributed to the revision of this paper. Q. Sun and W. W. Liu proposed the original idea and supervised the project. Z. Q. Yu and L. Sun contributed equally to this work.

Acknowledgments

This study was supported by the National Key R&D Program of China (2018YFB0504400), the National Natural Science Foundation of China (12061131010 and 12074198), the Russian Science Foundation (21-49-00023), and the Natural Science Foundation of Tianjin Municipality (20JCYBJCO1040).

References

[1] M. Kress, T. Löffler, S. Eden, M. Thomson, and H. G. Roskos, "Terahertz-pulse generation by photoionization of air with laser pulses composed of both fundamental and second-harmonic waves," *Optics Letters*, vol. 29, no. 10, pp. 1120–1122, 2017.

[2] M. Thomson, M. Kreß, T. Löffler, and H. G. Roskos, "Broadband THz emission from gas plasmas induced by femtosecond optical pulses: from fundamentals to applications," *Laser & Photonics Reviews*, vol. 1, no. 4, pp. 349–368, 2007.

[3] X. C. Zhang, A. Shkurinov, and Y. Zhang, "Extreme terahertz science," *Nature Photonics*, vol. 11, no. 1, pp. 16–18, 2017.

[4] X. Xie, J. M. Dai, and X. C. Zhang, "Coherent control of THz wave generation in ambient air," *Physical Review Letters*, vol. 96, no. 7, article 075005, 2006.

[5] K. Y. Kim, A. J. Taylor, J. H. Glownia, and G. Rodriguez, "Coherent control of terahertz supercontinuum generation in ultrafast laser–gas interactions," *Nature Photonics*, vol. 2, no. 10, pp. 605–609, 2008.

[6] M. Clerici, M. Peccianti, B. E. Schmidt et al., "Wavelength scaling of terahertz generation by gas ionization," *Physical Review Letters*, vol. 110, no. 25, article 253901, 2013.

[7] L. L. Zhang, W. M. Wang, T. Wu et al., "Observation of terahertz radiation via the two-color laser scheme with uncommon frequency ratios," *Physical Review Letters*, vol. 119, no. 23, article 235001, 2017.

[8] J. M. Dai, N. Karpowicz, and X. C. Zhang, "Coherent polarization control of terahertz waves generated from two-color laser-induced gas plasma," *Physical Review Letters*, vol. 103, no. 2, article 023001, 2009.

[9] Z. L. Zhang, Y. P. Chen, S. Cui et al., "Manipulation of polarizations for broadband terahertz waves emitted from laser plasma filaments," *Nature Photonics*, vol. 12, no. 9, pp. 554–559, 2018.

[10] H. L. Xu, A. Azarm, and S. L. Chin, "Controlling fluorescence from N_2 inside femtosecond laser filaments in air by two-color laser pulses," *Applied Physics Letters*, vol. 98, no. 14, article 141111, 2011.

[11] K. Y. Kim, J. H. Glownia, A. J. Taylor, and G. Rodriguez, "Terahertz emission from ultrafast ionizing air in symmetry-broken laser fields," *Optics Express*, vol. 15, no. 8, pp. 4577–4584, 2007.

[12] T. I. Oh, Y. S. You, N. Jhajj, E. W. Rosenthal, H. M. Milchberg, and K. Y. Kim, "Intense terahertz generation in two-color laser filamentation: energy scaling with terawatt laser systems," *New Journal of Physics*, vol. 15, no. 7, article 075002, 2013.

[13] H. M. Dai and J. S. Liu, "Terahertz emission dependence on the intensity ratio of 400-800 nm in generating terahertz waves from two-color laser-induced gas plasma," *Photonics and Nanostructures - Fundamentals and Applications*, vol. 10, no. 2, pp. 191–195, 2012.

[14] H. W. Du, M. Chen, Z. M. Sheng, and J. Zhang, "Numerical studies on terahertz radiation generated from two-color laser pulse interaction with gas targets," *Laser and Particle Beams*, vol. 29, no. 4, pp. 447–452, 2011.

[15] H. M. Dai and J. S. Liu, "Terahertz emission dependence on the irradiating laser pulse width in generating terahertz waves from two-color laser-induced gas plasma," *Journal of Modern Optics*, vol. 58, no. 10, pp. 859–864, 2011.

[16] H. M. Dai and J. S. Liu, "Terahertz emission dependence on the fundamental optical intensity in generating terahertz waves from two-color laser-induced gas plasma," *Chinese Physics Letters*, vol. 28, no. 10, article 104201, 2011.

[17] K. Y. Kim, "Generation of coherent terahertz radiation in ultrafast laser-gas interactions," *Physics of Plasmas*, vol. 16, no. 5, article 056706, 2009.

[18] S. Saxena, S. Bagchi, M. Tayyab et al., "Scaling up and parametric characterization of two-color air plasma terahertz source," *Laser Physics*, vol. 30, no. 3, article 036002, 2020.

[19] A. D. Koulouklidis, C. Gollner, V. Shumakova et al., "Observation of extremely efficient terahertz generation from mid-infrared two-color laser filaments," *Nature Communications*, vol. 11, no. 1, pp. 1–8, 2020.

[20] S. Saxena, S. Bagchi, M. Tayyab, J. A. Chakera, S. Kumar, and D. N. Gupta, "Enhanced broadband terahertz radiation from two-colour laser pulse interaction with thin dielectric solid target in air," *Journal of Infrared, Millimeter, and Terahertz Waves*, vol. 42, no. 7, pp. 747–760, 2021.

[21] Q. Sun, H. Jiang, Y. Liu, Z. Wu, H. Yang, and Q. Gong, "Measurement of the collision time of dense electronic plasma induced by a femtosecond laser in fused silica," *Optics Letters*, vol. 30, no. 3, pp. 320–322, 2005.

[22] S. S. Mao, F. Quéré, S. Guizard et al., "Dynamics of femtosecond laser interactions with dielectrics," *Applied Physics A*, vol. 79, no. 7, pp. 1695–1709, 2004.

[23] M. D. Feit and J. A. Fleck, "Effect of refraction on spot-size dependence of laser-induced breakdown," *Applied Physics Letters*, vol. 24, no. 4, pp. 169–172, 1974.

[24] C. A. Mancuso, K. M. Dorney, D. D. Hickstein et al., "Observation of ionization enhancement in two-color circularly polarized laser fields," *Physical Review A*, vol. 96, no. 2, article 023402, 2017.

[25] R. A. Kendall, T. H. Dunning, and R. J. Harrison, "Electron affinities of the first-row atoms revisited. Systematic basis sets and wave functions," *The Journal of Chemical Physics*, vol. 96, no. 9, pp. 6796–6806, 1992.

[26] A. D. Becke, "Density-functional thermochemistry. III. The role of exact exchange," *The Journal of Chemical Physics*, vol. 98, no. 7, pp. 5648–5652, 1993.